Welding in the World, 60, 2 (2016), 355–361.
doi:10.1007/s40194-015-0288-2

Qualitative and quantitative analyses of arc characteristics in SMAW

Masaya Shigeta*, Takahiro Ikeda**, Manabu Tanaka***, Tetsuo Suga***, Bovornchok Poopat****, Somporn Peansukmanee****, Niwat Kunawong****, Ackadech Lersvanichkool*****, Hiroaki Kawamoto*****, Supot Thongdee*****, Kazuyuki Suenaga******, Makoto Ota******

Abstract

This study was conducted to develop a quantitative evaluation system for arc characteristics such as arc stability and welding spatter generation related to shielded metal arc welding (SMAW) without human sensory evaluation. Factors that correspond to sensory evaluations by welders were investigated based on image processing. For the quantitative evaluation of arc stability, results show that the root mean square and the standard deviation of the arc center fluctuation, respectively, correspond to welders' sensory evaluation at AC and DC discharges. For welding spatter generation, a method of counting white pixels in a binarized image evaluates the number and size of welding spatters which closely coincide with welders' sensory evaluations.

Keywords

MMA welding; Electric arcs; Stability; Spatter; Sensors; Monitoring systems; Imaging

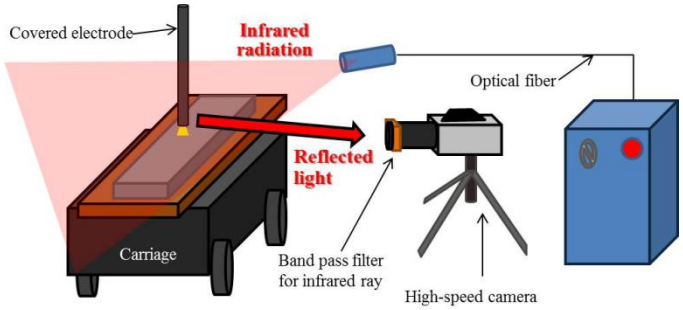

Fig. 1.
Lighting method for spatter measurement.

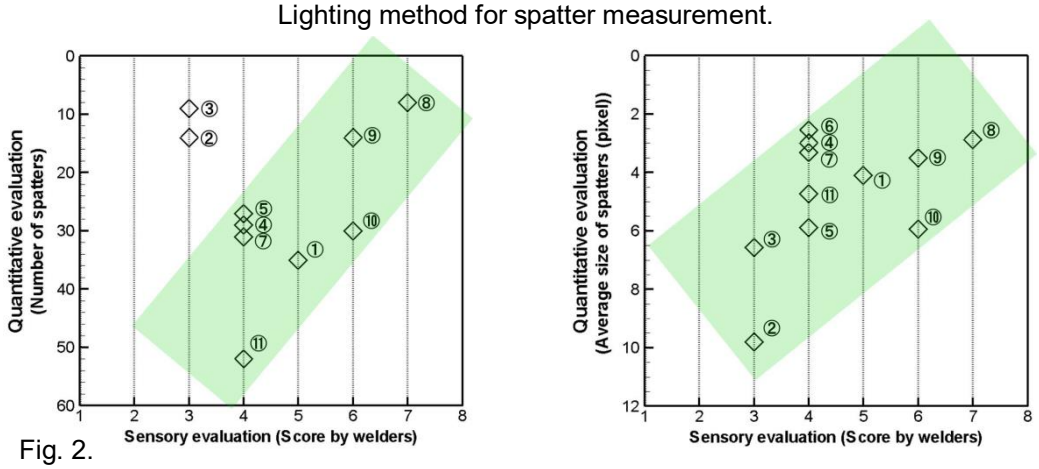

Fig. 2.
Correlation diagram between quantitative and sensory evaluations for welding spatters: (a) number of welding spatters and (b) size of welding spatters.

* Associate Professor
** Graduate School Student
*** Professor
**** King Mongkut's University of Technology Thonburi
***** Thai-Kobe Welding Co. Ltd.
****** Kobe Steel, Ltd.

Journal of Applied Physics, 120, 20 (2016), 203302.
doi: 10.1063/1.4968568

Effects of nonthermal plasma jet irradiation on the selective production of H_2O_2 and NO_2^- in liquid water

Giichiro Uchida*, Atsushi Nakajima**, Taiki Ito**, Kosuke Takenaka***, Toshiyuki Kawasaki****, Kazunori Koga*****, Masaharu Shiratani*****, Yuichi Setsuhara******

Abstract

We present the effects of the application of a nonthermal plasma jet to a liquid surface on H_2O_2 and NO_2^- generation in the liquid. Two distinct plasma irradiation conditions, with plasma contact and with no observable plasma contact with the liquid surface, were precisely compared. When the plasma was made to touch to the liquid surface, the H_2O_2 concentration of the plasma-treated water was much higher than the NO_2^- concentration. In contrast, when no observable contact of the plasma with the liquid surface occurred, the ratio of the NO_2^- to H_2O_2 concentration became over 1 and NO_2^- became more dominant than H_2O_2 in the plasma-treated water. Our experiments clearly show that reactive oxygen and nitrogen species can be selectively produced in liquid using appropriate plasma-irradiation conditions of the liquid surface. The ratio of NO_2^- to H_2O_2 was controlled within a wide range of 0.02 to 1.2 simply by changing the plasma-irradiation distance from the liquid surface.

Keywords

Nonthermal plasma jet; Plasma-liquid interaction; Reactive oxygen and nitrogen species

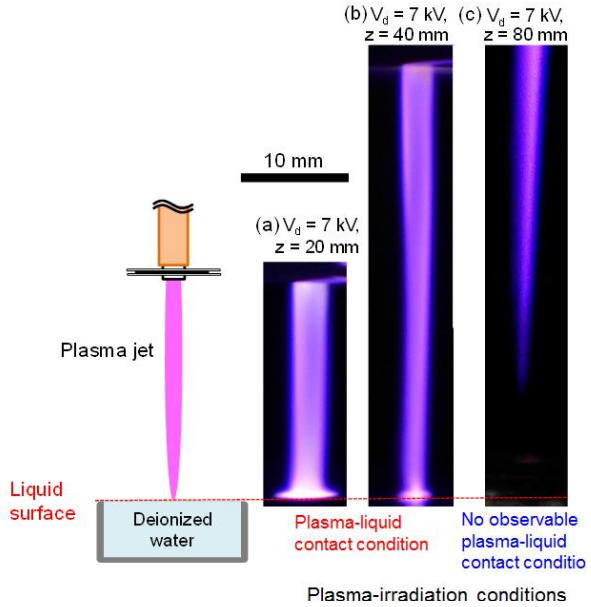

Fig.1.
Photographs of the plasma jet near the liquid surface at (a) z = 20 mm, (b) z = 40 mm, and (c) z = 80 mm. (a) and (b): plasma contact condition; (c): no observable plasma contact condition.

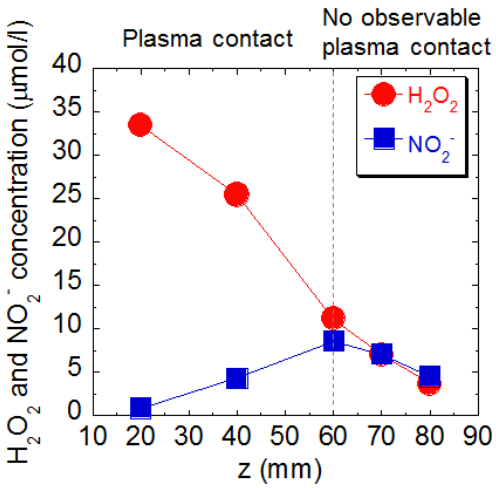

Fig.2.
z dependence of ratio of NO_2^- to H_2O_2 concentration in 3 mL of deionized water plasma-jet irradiated for 300 s.

* Associate Professor
** Graduate School Student
*** Assistant Professor
**** Nippon Bunri University
***** Kyushu University
****** Professor

Applied Physics A-Materials Science & Processing, 122-120, (2016), 1–4.
10.1007/s00339-016-9626-5

Cell spreading on titanium periodic nanostructures with periods of 200, 300 and 600 nm produced by femtosecond laser irradiation

M. Tsukamoto*, T. Kawa**, T. Shinonaga***, P. Chen****, A. Nagai****, T. Hanawa****

Abstract

Titanium (Ti) is an important biomaterial. We have used femtosecond laser irradiation to form periodic nanostructures on Ti plate for control of the cell spreading. In this study, periodic nanostructures with periodicities of 200, 300 and 600 nm were formed on a Ti plates using a femtosecond laser with wavelengths of 258, 388 and 775 nm, respectively. Cell spreading on the Ti plate for periodic nanostructures with periodicity of 200 nm lacked a definite direction, whereas cell spreadings on the Ti plate for periodic nanostructures with periodicities of 300 and 600 nm occurred along the grooves.

Keywords

Periodic nanostructure; Cell spreading; Femtosecond laser; Titanium; Biomaterial

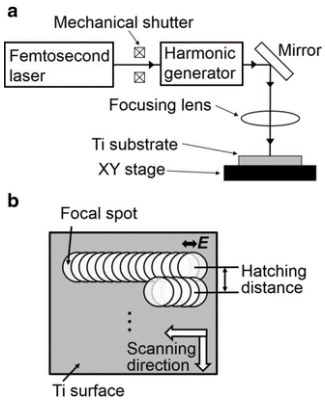

Fig. 1. Schematics of **a** the experimental setup for femtosecond laser irradiation of the Ti plate and **b** scanning direction of the femtosecond laser focal spot.

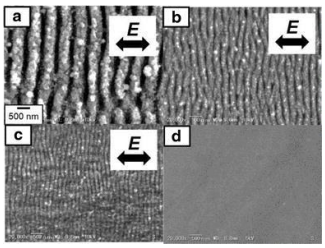

Fig. 3. SEM images of plates with periodic nanostructures formed by femtosecond laser irradiation at wavelengths of **a** 775 nm, **b** 388 nm and **c** 258 nm, and **d** a bare surface. The double-headed arrows indicate the laser electric polarization vector.

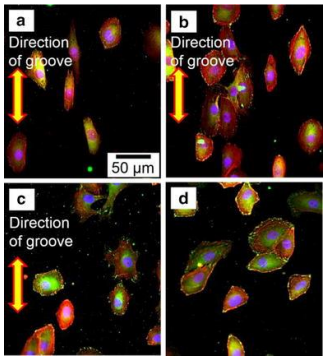

Fig. 5. Fluorescence microscope images of cells on plates with periodic nanostructures formed by femtosecond laser irradiation at wavelengths of **a** 775 nm, **b** 388 nm and **c** 258 nm, and **d** a bare surface.

* Associate Professor
** Graduate School Student
*** Faculty of Engineering, Okayama University
**** Institute of Biomaterials and Bioengineering, Tokyo Medical and Dental University

Quarterly Journal of the Japan Welding Society, 溶接学会論文集 34, 4 (2016), 239-248.

Relationship between melt flows based on three-dimensional X-ray transmission in-situ observation and spatter reduction by angle of incidence and defocusing distance in high-power laser welding of stainless steel

ステンレス鋼の高出力レーザ溶接における 3 次元 X 線透視その場観察による湯流れと入射角および焦点はずし距離によるスパッタ抑制との関係

Yousuke Kawahito*, Kouki Nakada**, Yousuke Uemura**,
Masami Mizutani***, Kouji Nishimoto****, Hiroshi Kawakami*****,
Seiji Katayama******

川人洋介*, 中田光紀**, 上村洋輔**, 水谷正海***, 西本浩司****, 川上博士*****,
片山聖二******

Abstract

The objective of this research is to reveal relationship between melt flows and spatter reduction by angle of incidence and defocusing distance in partial-penetration welding of a SUS304 stainless steel plate with a 6-kW power laser beam. In welding speeds from 50 mm/s to 250 mm/s, underfilled weld beads with spatters were obtained more than 150 mm/s. Accoriding to three-dimensional X-ray transmission in-situ observation of melt flows at 150 mm/s in welding speed with tungsten carbide (WC) tracers, the melt flews achieved approximately 2.3 m/s in speed and made convex molten-pool surface behind a keyhole inlet grow higher, resulting in spattering over 0.1 mm in the diameter. A 2-mm inner defocusing distance or a 20-degrees angle of advance decreased the number of spatter over 0.1 mm in the diameter by half or one third in comparison with that at focal point and zero angles. The X-ray transmission images demonstrate that the appropriate defocusing distance and angle of incidence made the speed of the melt flow decrease and the melt flow behind a keyhole inlet circulate, which led to not only suppressing the convex surface but also improving the frequency that the convex surface went back to the molten pool.

Keywords

Spatter; Melt flow; Laser welding; Three-dimensional X-ray transmission in-situ observation

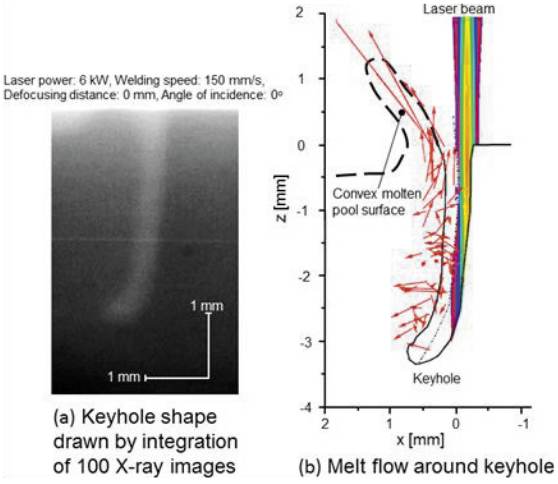

Fig. 1. Keyhole shape and two dimensional melt flows around keyhole at focal point.

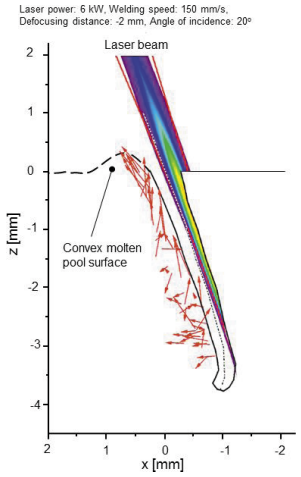

Fig. 2. Two dimensional melt flows at both defocusing distance of -2 mm and 20 degrees angle of advance.

*	Associate Professor	*****	Mie University
**	Graduate School Student	******	Guest Professor
***	Senior Technical Specialist (Technical Expert Division)		
****	Anan National College of Technology		

Materials and Design, 110, (2016), 888–894.
doi: 10.1016/j.matdes.2016.08.060

Direct solid-state diffusion bonding of zirconium carbide using a spark plasma sintering system

Kazuyuki Kohama*, Kazuhiro Ito**

Abstract

The authors conducted direct solid-state diffusion bonding of zirconium carbide (ZrC)-sintered materials with different average grain sizes of 3.5, 7.5 and 35 μm using a spark plasma sintering system. ZrC samples were bonded at 1300–2000 °C for 20 min with no defects or oxidation. Shear tests on the ZrC–ZrC joints at room temperature revealed that the bonding temperature to obtain joints with a strength at the bonding interface that is higher than the fracture strength of the base materials could be reduced by reducing the ZrC average grain size. Microstructure studies around the bonding interface showed that the bonding process was controlled by grain-boundary diffusion, and the dominant driving force was a lowering boundary energy at the intersection of the grain boundary and the bonding interface (i.e., triple junctions at the bonding interface). Grain boundary migration across the bonding interface at the triple junctions was suggested to increase joint strength. The higher density of the triple junctions derived from the reduced ZrC grain size is thought to enhance grain boundary migration and increase the driving force and diffusion paths for grain boundary diffusion, which results in the formation of joints with a higher bonding interface strength.

Keywords

Refractory ceramic material; Transition-metal carbide; Shear strength; Fine microstructure; Electron backscattering diffraction analysis

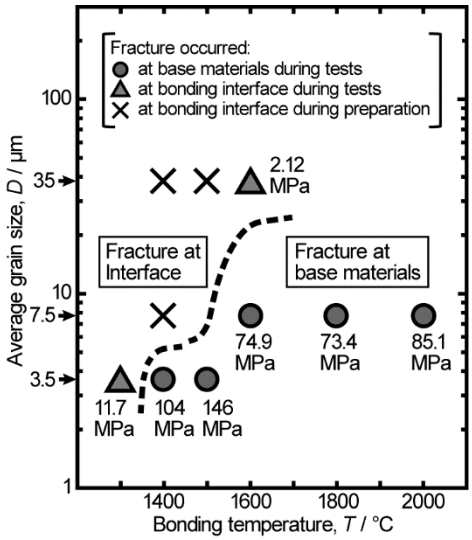

Fig. 1. Summary of results of shear tests for ZrC–ZrC joints.

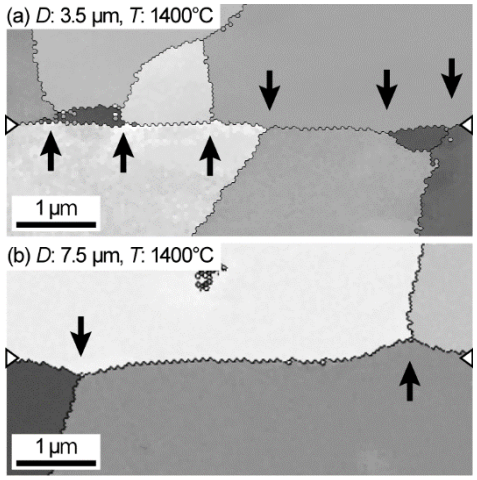

Fig. 2. Cross-sectional EBSD images around bonding interface for ZrC–ZrC joints bonded at 1400°C with average grain size of (a) 3.5 μm and (b) 7.5 μm.

* Assistant Professor
** Professor

Research Division of Materials Joining Mechanism, Dep. of Joint Interface Structure and Formation Mechanism

Materials and Design, 90, (2016), 915–921.
http://dx.doi.org/10.1016/j.matdes.2015.11.037

Stabilization of austenite in low carbon Cr-Mo steel by high speed deformation during friction stir welding

Takuya Miura*, Rintaro Ueji**, Hidetoshi Fujii***, Hisanao Komine****, Jun Yanagimoto****

Abstract

Friction stir welding (FSW) was applied to a low carbon alloyed steel in order to stabilize the austenite phase which can effectively maintain a preferable toughness. A Cr–Mo steel sheet (0.20 wt.%C–1.07%Cr–0.16%Mo–0.24%Si–0.61%Mn–bal. Fe) with a ferrite pearlite structure was friction stir welded under the conditions in which the sample was reheated above the A_3 temperature at the maximum. The microstructure observations in the stir zone clarified martensite with several area fractions of retained austenite and elongated ferrite. The retained austenite provides a high ductility with a high strength in the stir zone. In order to clarify the formation mechanism of the austenite, compression tests were conducted at various strain rates up to 10/s using an ultrahigh-speed compression testing machine. When the sample was compressed at the high strain rate, the elongated ferrite grains and retained austenite were formed. This microstructure was similar to the microstructure in the FSW stir zone, suggesting that the efficient accumulation of plastic strain in the austenite during the FSW plays an important role in obtaining the retained austenite.

Keywords

Friction stir welding; Steel; Strain rate; Phase transformation

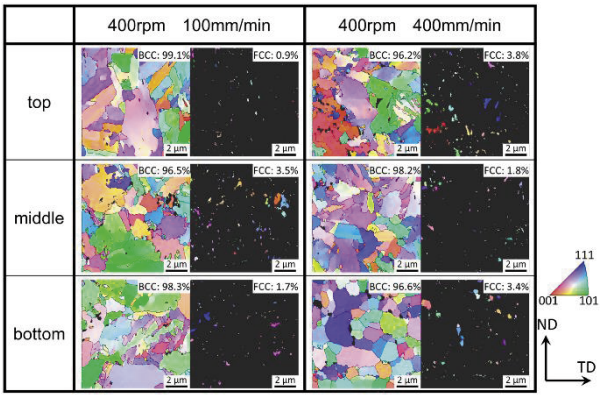

Fig. 1. Orientation color maps in the stir zones of SCM420 welded at the tool rotation speed of 400 rpm and the welding speeds of 100 mm/min and 400 mm/min. The crystal orientations parallel to the WD are separately indicated by the color of the normal stereo triangle within the BCC and FCC.

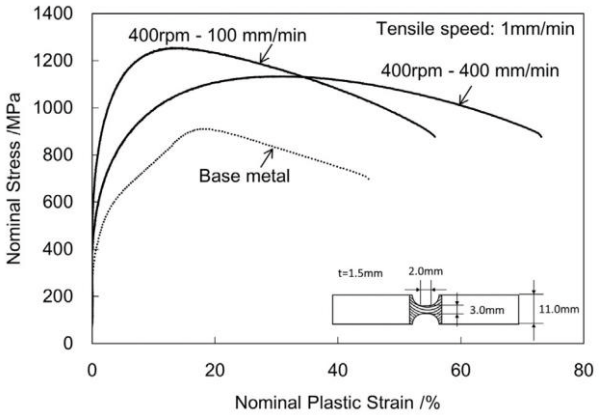

Fig. 2. Nominal stress–nominal plastic strain curves of the base metal and stir zones of SCM420 welded at the tool rotation speed of 400 rpm and the welding speeds of the 100 mm/min and 400 mm/min. The shape of the test piece is shown on the right bottom side.

* Graduate school student
** Associate Professor
*** Professor
**** Institute of Industrial Science, The University of Tokyo

Scripta Materialia, 113, (2016), 158–162.
doi:10.1016/j.scriptamat.2015.11.011

Simultaneously enhancing strength and ductility of carbon nanotube/aluminum composites by improving bonding conditions

Biao Chen*, Katsuyoshi Kondoh**, Hisa Imai***, Junko Umeda***, Makoto Takahashi****

Abstract

The limited ductility of high-strength aluminum (Al) matrix composites (AMCs) reinforced with carbon nanotubes (CNTs) is a critical issue, which hinders their engineering applications. Here, it was clarified that a significantly improved ductility of CNT/Al composites with a simultaneously increased tensile strength using elevated sintering temperatures. The traditional trade-off tendency between strength and ductility was evaded in CNT/Al composites owing to concurrent improvement of Al–Al grains and CNT–Al interface bonding. The interfacial characteristics were investigated through microstructural examination analysis and quantitative estimation using the strengthening models. The study obviously provided a strategy for fabricating CNT-reinforced metal matrix composites with high strength and good ductility. For example, the elongation of CNT/Al composite sintered at 900 K was enhanced 82% comparing with that sintered at 800 K, while an increment of 18% in YS was achieved, as well as 14% in UTS.

Keywords

Metal matrix composite (MMC); Carbon nanotubes (CNTs); Strength; Ductility; Bonding

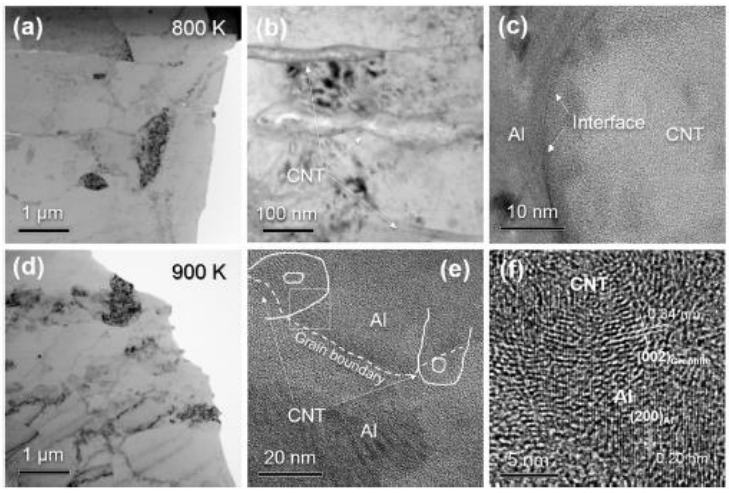

Fig. 1. TEM observation on CNTs/Al composites sintered at 800K (a-c) and 900K (d-f) at different magnifications. (a, b, d, e) are views on CNTs in Al matrix, and (c, f) are HR-TEM observation results of CNT-Al interface.

* Specially Appointed Researcher
** Professor
*** Assistant Professor
**** Associate Professor

Welding in the World, 60, 5 (2016), 1037–1046.
doi: 10.1007/s40194-016-0360-6

Finite element analysis of deformation in early stage of multi-pass circumferential dissimilar welding of thick-walled pipes with narrow gap

Hisashi Serizawa*, Yusuke Okuda**, Hidekazu Murakawa***

Abstract

Three-dimensional thermal elastic-plastic finite element analyses were conducted in order to reveal the mechanism of gap shrinkage in early stage of multi-pass narrow gap welding of thick-walled dissimilar pipes and thick plates. The gap shrinkage up to the 8th pass indicates that the shrinkage of plates becomes to be much larger than that of pipes with increasing the weld passes. In addition, through the decomposition of gap shrinkage to transverse shrinkage and angular distortion, it is found that the gap shrinkage of pipes is mainly governed by the transverse shrinkage, while the shrinkage of plates is influenced by both the transverse shrinkage and angular distortion. Moreover, the serial computational results with various groove shapes suggest that the transverse shrinkage of pipes almost linearly increases with increasing the weld pass, and its increment can be predicted by a linear approximation function obtained by the transverse shrinkage of plates regardless of the groove shape.

Keywords

Gap; Multirun welding; Distortion; Transverse shrinkage; Finite element analysis; Circumferential welds; Dissimilar materials; Tubes and pipes

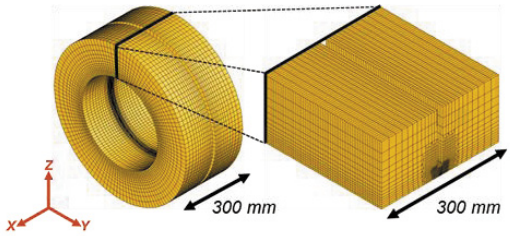

Fig. 1. Finite element models of butt-welded and plates.

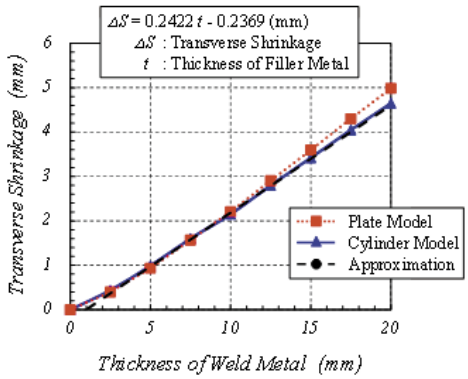

Fig. 2. Approximation of transverse shrinkage during multi-pass welding of butt-welded pipes based on butt-welded plates.

* Associate Professor
** Graduate School Student
*** Professor

Welding in the World, 60, 6 (2016), 1191–1199.
doi:10.1007/s40194-016-0383-z

Evaluation of Charpy impact toughness using side-grooved specimen for hybrid laser-arc welds of ultra-high-strength steel

Yasuhito Takashima*, Mitsuru Ohata**, Koutarou Inose***,
Hiroto Yamaoka***, Yasumasa Nakanishi***, Fumiyoshi Minami****

Abstract

This paper discusses the significance of a narrow hard weld bead, produced by hybrid laser-arc welding, on the Charpy absorbed energy. A parametric finite element analysis with various strength mismatching and bead widths has been conducted on the strain field of side-grooved and normal Charpy specimens. The narrow weld bead promotes the accumulation of plastic strain energy on the base metal side. This feature is more significant in the normal specimen than in the side-grooved specimen. The results show that the method based on the Weibull stress criterion for converting the absorbed energy of the side-grooved specimen to that of the normal specimen can be applied to hybrid laser-arc welds of ultra-high-strength steel. The converted energy is consistent with the absorbed energy measured in the normal specimen. This study indicated that the absorbed energy of side-grooved specimen corresponding to the absorbed energy of the normal V-notch specimen increases with increasing hard zone width. On the other hand, the influence of strength mismatch ratio on the difference of the absorbed energy is rather weak.

Keywords

Hybrid laser arc welding; Impact toughness; Brittle fracture; Mismatch; Structural steels

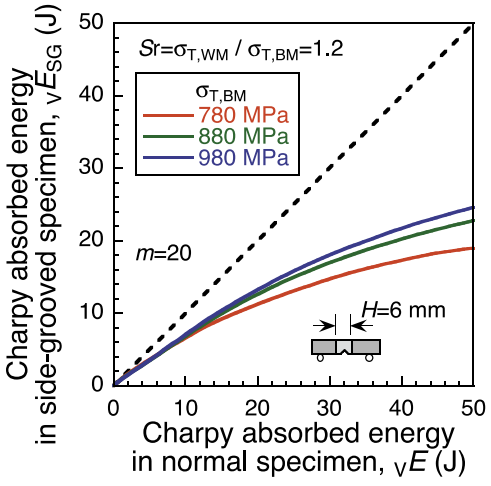

Fig. 1.
Influence of strength of base metal on the relation between $_vE$ and $_vE_{SG}$ at which the specimens sustain the same magnitude of Weibull stress for Sr = 1.2.

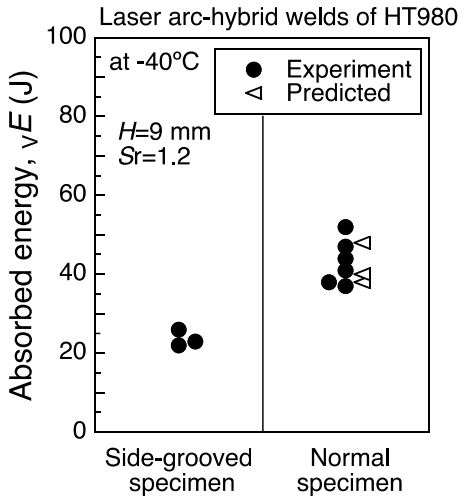

Fig. 2.
Comparison of Charpy absorbed energy measured and converted from the absorbed energy of the side-grooved specimen of the welds of HT980 steel at −40 °C.

* Assistant Professor
** Osaka University
*** IHI Corporation
**** Professor

Fracture and Structural Integrity, 38, (2016), 240–250.
doi: 10.3221/IGF-ESIS.38.33

Fatigue life assessment of a non-load carrying fillet joint considering the effects of a cyclic plasticity and weld bead shape

Seiichiro Tsutsumi*, Kasumi Morita**, Riccardo Fincato***, Hideto Momii**

Abstract

Fatigue life depends strongly on irreversible contributions that accumulate during cyclic loading and unloading of structures. However, the correct identification of the loading path in terms of uniaxial or multi-axial stress states, proportional or non-proportional loading is essential because these factors can significantly alter the material response. In this study, finite element analysis is conducted to assess the fatigue crack initiation life of a non-load carrying fillet joint by considering weld bead shape and a cyclic plasticity accumulation during fatigue loading, which is a main cause of crack initiation. Cyclic plasticity behavior including cyclic hardening and softening together was investigated with an unconventional plasticity model called the subloading surface model and extended to include both elastic boundary and cyclic damage concepts. The cyclic plasticity model can capture realistic plastic strain accumulation during high cycle fatigue under macroscopically elastic stressing conditions.

Keywords

Composite materials; Unconventional plasticity; Fatigue; Loading path; Crack initiation

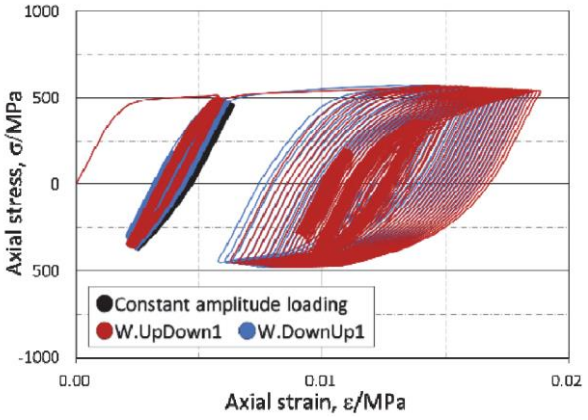

Fig..

Stress-strain curves at element A (constant amplitude loading/variable loading).

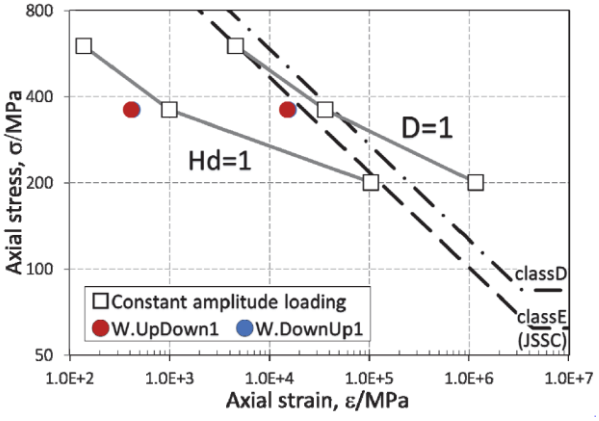

Fig..

S-N curves at element A (constant amplitude loading/variable loading).

* Associate Professor
** Graduate School Student
*** Specially Appointed Researcher

Research Division of Materials Joining Assessment, Dep. of Reliability Evaluation & Simulation

Proceedings of the Visual-JW2016, 1, (2016), 119–120.

Fundamental study on intragranular transformation mechanism in low alloy steel weld metal

Suo Saruwatari*, Kazuhiro Kojima*, Hiroyuki Hirata*, Hiroshige Inoue**

Abstract

To improve the toughness of low alloy steel weld metal, the fine transformation structures such as acicular ferrite are effective. Acicular ferrite is generated with inclusions as its nucleation sites. So, we have tried to reveal the structure of the inclusions being the initiation sites and the formation mechanism of them. Amorphous Al-Mn-Si-Oxide was observed at the outside of crystalline (Mn, Ti) Al_2O_4 that formed in the central part of inclusions. At the outermost layer of the inclusions, titanium compound layer covered inclusions and the layer of about 10 nm was identified as Ti (N, O). This Ti (N, O) was the initiation sites generating acicular ferrite. To examine at what stage of the weld cooling the inclusions of this structure were formed, the inclusions in the weld metal that was frozen by liquid tin quenching method during welding were analyzed. In the molten metal, Ti hardly covered on the surface layer of inclusions. However, in the weld metal cooled up to around 1273K, the Ti (N, O) layer was confirmed at the outermost layer of inclusions.

Keywords

Arc welding; Low alloy steel; Intragranular transformation; Acicular ferrite; Inclusion

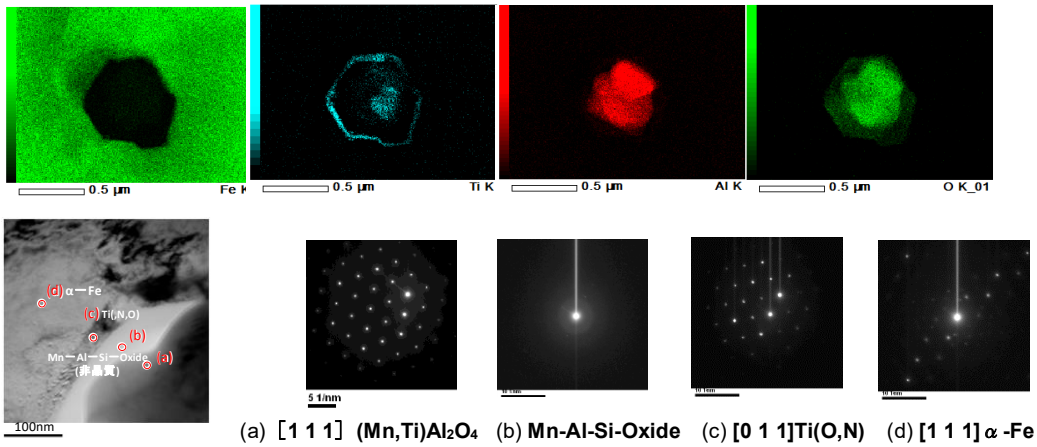

Fig. 1. TEM analysis results of the inclusion in weld metal.

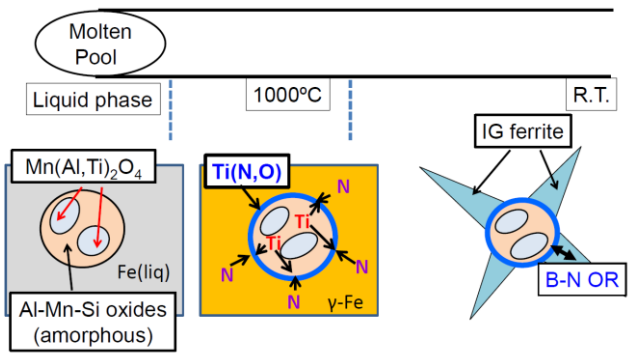

Fig. 2. Schematic illustration of the formation mechanism of the inclusions in weld metal.

* Nippon Steel & Sumitomo Metal Corporation
** Professor

Journal of Power Sources, 320, (2016), 120–126.
doi:10.1016/j.jpowsour.2016.04.086

Insertion of lattice strains into ordered $LiNi_{0.5}Mn_{1.5}O_4$ spinel by mechanical stress: A comparison of perfect versus imperfect structures as a cathode for Li-ion batteries

Takahiro Kozawa*, Takeshi Murakami**, Makio Naito***

Abstract

The Ni-doped lithium manganese oxide, $LiNi_{0.5}Mn_{1.5}O_4$, has received much attention as a cathode material in high-energy lithium-ion batteries (LIBs). This active material has two different spinel structures depending on the ordering state of the Ni and Mn ions. The ordered $LiNi_{0.5}Mn_{1.5}O_4$ spinel has an inferior cathode performance than the disordered phase because of its poor electronic conductivity. However, the ordered $LiNi_{0.5}Mn_{1.5}O_4$ spinel possesses the potential advantage of avoiding dissolution of the Mn ion, which is an issue for the disordered spinel. The improvement of cathode performance is important for future applications. Here, we report a unique approach to improve the cathode performance of the ordered $LiNi_{0.5}Mn_{1.5}O_4$ spinel. The mechanical treatment using an attrition-type mill successfully inserted lattice strains into the ordered $LiNi_{0.5}Mn_{1.5}O_4$ spinel structure without a phase transformation to the disordered phase. The insertion of lattice strains by mechanical stresses provided an increased discharge capacity and a decreased charge transfer resistance. This limited crystal structure modification improved the cathode performance.

Keywords

Lattice strain; Mechanical stress; $LiNi_{0.5}Mn_{1.5}O_4$; Spinel; Cathode; Li-ion battery

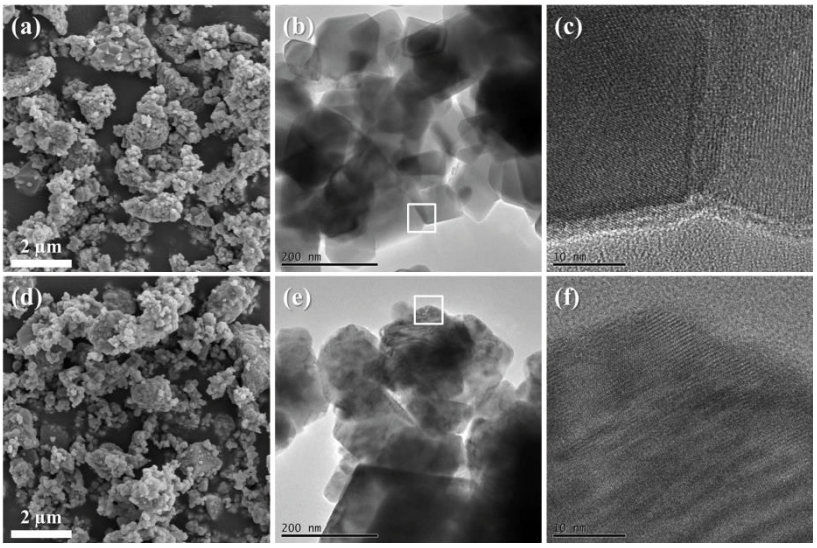

Fig.1.

FE-SEM and HR-TEM images of (a-c) p-LNMO and (d-f) MT20-LNMO particles.

* Assistant Professor
** Technical Assistant, Technical Expert Division
*** Professor

Welding in the World, 60, 4 (2016), 697–702.

Additive manufacturing of ceramic components using laser scanning stereolithography

Soshu Kirihara*

Abstract

Three-dimensional stereolithographic additive manufacturing was customized successfully to create ceramics components with functional microstructures. Photosensitive acrylic resins with titania or alumina nanoparticles were spread on a glass substrate with a mechanical knife edge. Two-dimensional patterns formed by ultraviolet laser scans of 10 to 100 μm in diameter were laminated to create composite precursors. Dense components could be obtained through dewaxing and sintering of the composite. Photonic four-coordinate crystal lattices with periodic arrangements of the dielectric constant were created to control electromagnetic waves in the gigahertz and terahertz frequency ranges by Bragg diffraction. Systematic optimization of the stereolithographic lamination and heat treatment patterns will be investigated to improve the dielectric microstructures related to the microwave properties.

Keywords

Additive manufacturing; Ceramics; Stereolithography

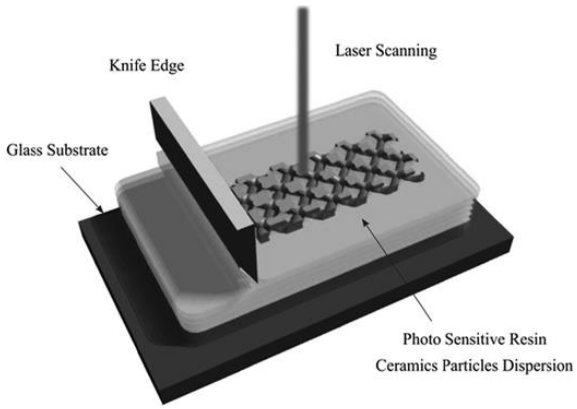

Fig. 1.
Schematic illustration of 3D stereolithographic additive manufacturing using photosensitive resin pastes with ceramic nanoparticle dispersions. Composite precursors could be created by laminating 2D cross sections drawn by laser scanning.

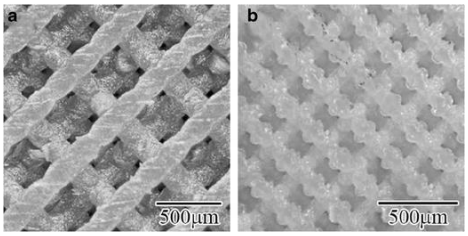

Fig. 4.
Fully ceramic components of the photonic crystals processed by the dewaxing and sintering treatments of the composite precursors: diamond-structured titania (a) and alumina (b) micropatterns with lattice constants of 720 and 350 μm, respectively.

* Associate Professor

Scripta Materialia, 120, (2016), 80–84.
doi:10.1016/j.scriptamat.2016.04.018

Low-pressure Cu-Cu bonding using in-situ surface-modified microscale Cu particles for power device packaging

Xiangdong Liu*, Hiroshi Nishikawa**

Abstract

Since Pb-containing solders are currently being used for die-attach bonding in power device packaging, a number of investigations are targeted towards finding suitable Pb-free high temperature bonding. An oxidation-reduction bonding (ORB) was applied to achieve Cu-Cu bonding with microscale Cu particle paste. During sintering at 300 °C, Cu_2O nanoparticles were homogeneously formed on the surface of the microscale Cu particles through a thermal oxidation, and were subsequently reduced to Cu nanotextured surface in formic acid atmosphere. This in-situ surface modification significantly enhances the sinterability of the microscale Cu particles, leading to a well-sintered microstructure and a three times higher bonding strength than that of the bonding joints prepared with non-oxidation bonding (NOB).

Keywords

Pb-free high temperature bonding; Sintering; Surface modification; Copper; Oxidation-reduction bonding

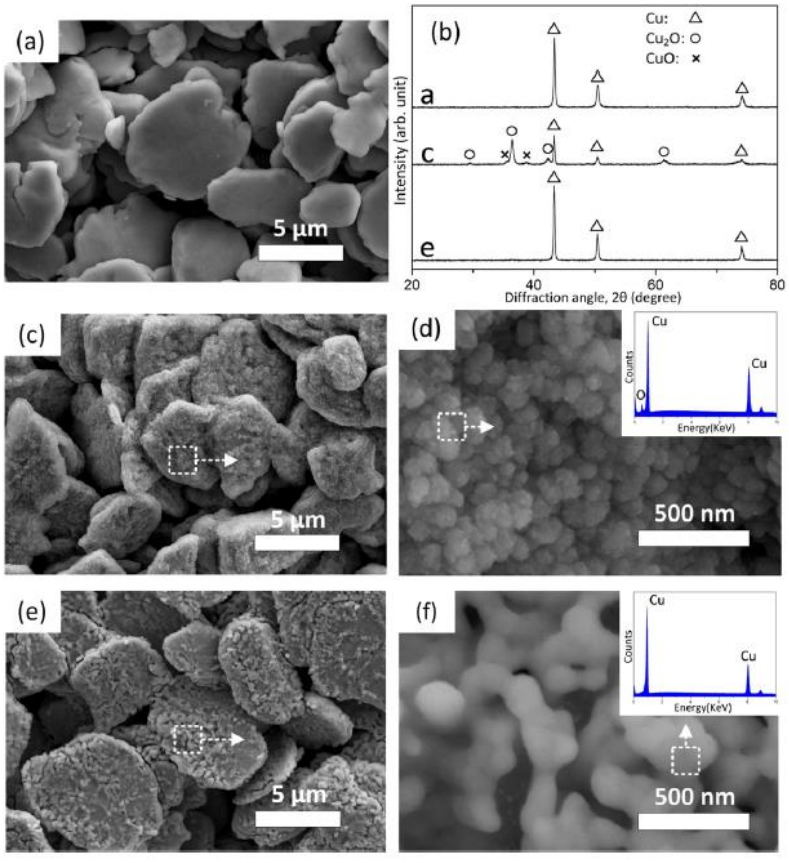

Fig. 1. FE-SEM images, corresponding EDX spectra and XRD patterns of the Cu particles. (a) after heating at 300 °C for 60min in formic acid atmosphere, (c, d) after heating at 300 °C for 20 min in air, (e, f) after heating at 300 °C for 20 min in air followed by heating at 300 °C for 5 min in formic acid atmosphere, (b) XRD patterns of the particles in (a), (c) and (e).

* Graduate School Student
** Associate Professor

Proceedings of 10th International Conference on Trends in Welding Research & 9th International Welding Symposium of Japan Welding Society (9WS), (2016), 136–139.

Application to duplex stainless steel of narrow gap oscillation laser welding

Yohei Abe*, Yosuke Yamazaki**, Yukio Hioki**, Mitsuyoshi Nakatani***, Akikazu Kitagawa****

Abstract

The narrow gap welding process can reduce the groove section area drastically compared to other welding processes, achieving a weld joint with low heat input and resulting in minimal distortion. In our group, the narrow gap oscillation laser welding using high power laser as heat resource has been studied. This process uses a high-power laser as its heat source and oscillates it rapidly. Setting the control of the center of laser beam oscillation and the laser beam oscillation width to adjust the groove's position and width can be expected to prevent the lack of fusion on the groove side wall often occurring in narrow gap arc welding. This research establishes the narrow gap oscillation laser welding process for plate butt welding of duplex stainless steel, and establishes a laser multi-layer welding system in order to apply to actual production.

Keywords

Laser welding; Oscillation laser; Multi-layer welding; Duplex stainless steel

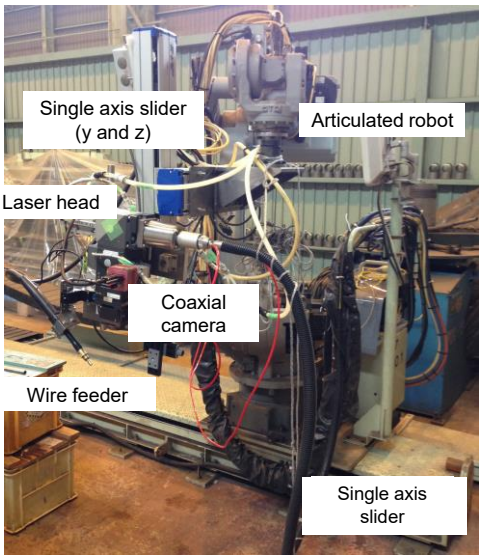

Fig. 1.
Overview of Multi-layer welding system.

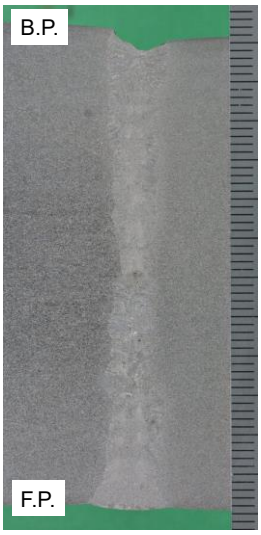

Fig. 2.
Overview of Multi-layer welding system.

* Specially Appointed Assistant Professor
** Hitachi Zosen Corporation
*** Specially Appointed Associate Professor
**** Guest Professor

Radiation Oncology, 11, 1 (2016), 91.
doi: 10.1186/s13014-016-0666-y

Titanium peroxide nanoparticles enhanced cytotoxic effects of X-ray irradiation against pancreatic cancer model through reactive oxygen species generation *in vitro* and *in vivo*

Masao Nakayama*, Ryohei Sasaki*, Chiaki Ogino*, Tsutomu Tanaka*, Kenta Morita*, Mitsuo Umetsu**, Satoshi Ohara***, Zhenquan Tan****, Yuya Nishimura*, Hiroaki Akasaka*, Kazuyoshi Sato*****, Ciya Numako******, Seiichi Takami**, Akihiko Kondo*

Abstract

Biological applications of nanoparticles are rapidly increasing, which introduces new possibilities to improve the efficacy of radiotherapy. Here, we synthesized titanium peroxide nanoparticles (TiOxNPs) and investigated their efficacy as novel agents that can potently enhance the effects of radiation in the treatment of pancreatic cancer. TiOxNPs and polyacrylic acid-modified TiOxNPs (PAA-TiOxNPs) were synthesized from anatase-type titanium dioxide nanoparticles (TiO_2NPs). The TiOxNPs and PAA-TiOxNPs showed a distinct ability to produce hydroxyl radicals in response to X-ray irradiation in a dose- and concentration-dependent manner, whereas the TiO_2NPs did not. At the highest concentration of TiOxNPs, the amount of hydroxyl radicals increased by >8.5-fold following treatment with 30 Gy of radiation. The absorption of PAA-TiOxNPs enhanced DNA damage and resulted in higher cytotoxicity in response to X-ray irradiation in vitro. The combination of the PAA-TiOxNPs and X-ray irradiation induced significantly stronger tumor growth inhibition compared to treatment with either PAA-TiOxNPs or X-ray alone ($p < 0.05$) as shown in Fig.1. No apparent toxicity or weight loss was observed for 43 days after irradiation.

Keywords

Nanopaticles; Titanium peroxide; Radiation; Reactive oxygen species; Pancreatic cancer

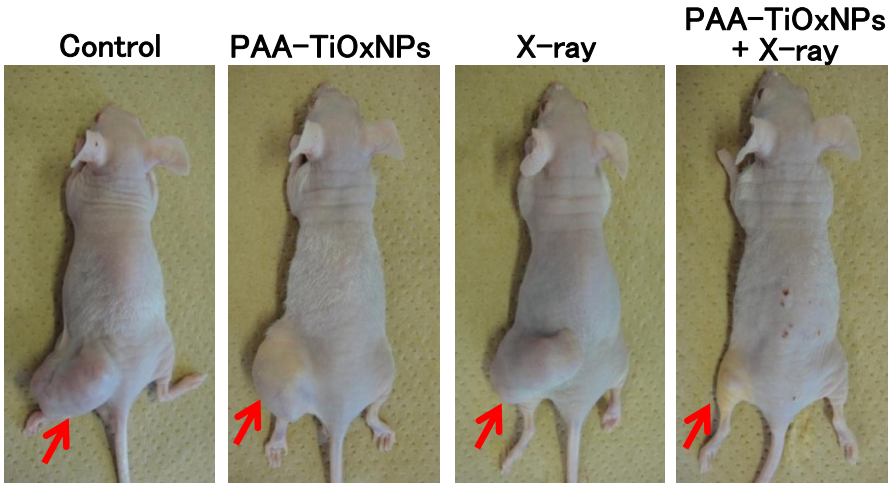

Fig. 1.
Tumor growth-inhibitory effects of PAA-TiOxNPs combined with X-ray radiation.
Tumor appearance in the xenografts for each treatment after 43 days.

* Kobe University
** Tohoku University
*** Specially Appointed Professor
**** Dalian University of Technology
***** Gunma University
****** Chiba University

Activity report on “The Project to Create Research and Educational Hubs for Innovative Manufacturing in Asia”

Mihoko Katsumata*, Futoshi Himi **, Yosuke Kawahito ***
勝又　美穂子、氷見　太、川人　洋介

Abstract

In this project, three pillars were set; 1) Establish a global network of researchers in joining technologies across Greater Asia Region, 2) Develop new key technologies for joining adaptable to extreme environments, 3) Implement oversea internships which tie up students from area of science and the humanities, named as Coupling internships (CIS). Based on these pillars, activities implemented this year were reported as below.

1) Total of 8 international joint researches were implemented including 3 newly commenced and 5 continuous researches from previous years. 2 workshops with Nanyang Technological University, Indonesia University respectively, and one annual symposium invited domestic and oversea speakers were organized. International joint research overviews are listed in Table 1.
2) Research on Underwater Laser Welding Technology were continued to develop laser welding torch while pursuing the optimal operation circumstances at underwater.
3) Coupling Internship was implemented in 5 different countries which were in Indonesia, Vietnam, Thailand, Myanmar, and in Singapore. Pictures from CIS can be found in Fig. 1 and Fig. 2.
4) Based on the networks made, JWRI received 18 students in total from partner universities in Taiwan, Thailand, India, Vietnam and Indonesia under JST Sakura Science Plan.

Partner University	Research Topics
King Mongkut's University of Technology, Thonburi (Thailand)	Advanced high-strength titanium powder metallurgy materials for medical devices
National Metal and Materials Technology Center (Thailand)	Research on laser welding for joining of open-cell aluminum with solid shell
Istanbul Technical University (Turkey)	The predictions of residual distortions caused by welding/welding methodologies and productions methods in shipbuilding
National Metal and Materials Technology Center (Thailand)	Stereolithographic additive manufacturing of biomaterials implants
Indian Institute of Technology, Hyderabad (India)	Relationship between mechanical properties and microstructure of welds in Twin-wire GMAW welding of low carbon steel
Nanyang Technological University (Singapore)	Residual stress modeling and fatigue life prediction in cladding specimen and welded pipe
Indian Institute of Technology, Hyderabad (India)	Research on the melting phenomenon in waveform-controlled SAW
Malaya University (Malaysia)	Assessments of FSW dissimilar joints between steel and Mg with addition of powder filler

Table 1 List of International Joint Research in 2016.

Fig. 1. Pictures from CIS Singapore.

Fig. 2. Pictures from CIS Vietnam.

* Specially Appointed Associate Professor
** Specially Appointed Researcher
*** Associate Professor

ISIJ International, 56, 7 (2016), 1226–1231.
http://doi.org/10.2355/isijinternational.ISIJINT-2016-042

Friction lap joining of thermoplastic materials to carbon steel

Kimiaki Nagatsuka*, Daiki Kitagawa**, Hiroto Yamaoka***, Kazuhiro Nakata****

Abstract

Dissimilar material joining of polyamide 6 and polyethylene plates to a plain carbon steel (SPCC) plate was performed using friction lap joining. The polyamide 6 and SPCC plates could be directly joined by friction lap joining, whereas the polyethylene and SPCC plates could not. Corona discharge treatment of the polyethylene surface enabled the joint formation with SPCC. The tensile shear fracture load of the SPCC/polyamide 6 and SPCC/corona-discharge-treated polyethylene joints increased with the joining speed up to 600 mm min^{-1}, beyond which it decreased. These joints were fractured at the base material of the plastic plate at optimal joining speeds in the tensile shear test. Continuously joined interfaces of these materials were observed via cross-sectional microstructure analysis. Transmission electron microscopy and selected area diffraction patterns indicated that these materials were joined through the surface oxide layer of SPCC composed of Fe_3O_4. The relation between the tensile shear fracture loads and the results of XPS analysis indicated that polar groups such as amide, hydroxyl, and carboxyl groups on the plastic surfaces were highly effective for joint formation of the SPCC/plastic joints.

Keywords

Friction lap joining; Plain carbon steel; Polyamide 6; Polyethylene; Corona discharge treatment; Polar group; Dissimilar material joining

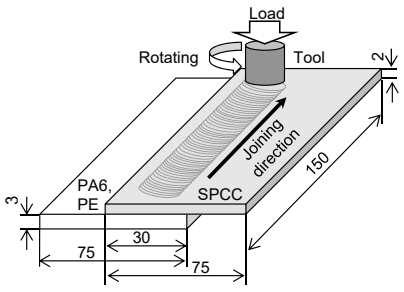

Fig. 1.
Schematic illustration of friction lap joining for the plastic to the metal (all dimensions in mm).

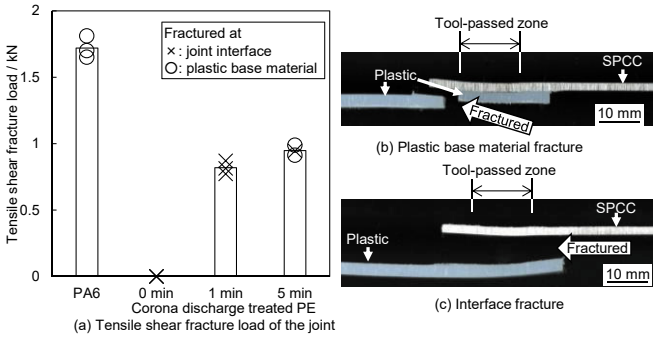

Fig. 2. (a) Tensile shear fracture load of FIJ joints of SPCC/PA6, as-received and corona-discharge treated PE processed at the joining speed of 600 mm min^{-1}, and the joint appearances fractured at (b) the plastic base plate and (c) the joint interface.

* Specially Appointed Assistant Professor
** Graduate School Student
*** IHI Corporation
**** Specially Appointed Professor

Proceedings of 23rd MATE 2017, (2017), 305–308.

The influence of oxygen diffusion path at carbon cathode on electrochemical discharge performance in Mg-air batteries

Zhonghao Heng*, Shigeaki Uchida**, Yasuo Takahashi***

Abstract

In order to design series stacked magnesium-air batteries for high power source, the diffusion path of oxygen for cathode reaction in layered battery is experimentally investigated. The electrochemical discharge performance of single unit Mg-air cell using carbon cathode is measured in terms of output power. The results show that both parallel and perpendicular air flow can work on the cathode reaction. Discharge performance is maintained approximately 65% when the air flow diffused through the carbon cathode is blocked. The peak power can reach to 85 mW under the conditions of parallel air flow is enough, initial water supply is 1.0 g and electrode area is 25 mm×50 mm. The peak output power reduces when the parallel air flow is impeded. Initial power reduction so called “battery flooding”, a phenomenon that occurs with excess water supply to batteries, is observed. Adequate conditions of water supply and air flow are essential for obtaining good discharge performance of Mg-air battery.

Keywords

Magnesium air battery; Carbon cathode; Oxygen reduction reaction; Diffusion path; Discharge performance

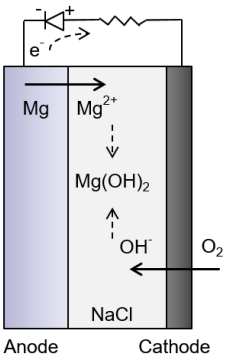

Cathode: $O^2 + 2H_2O + 4e^- \rightarrow 4OH^-$

Anode: $2Mg \rightarrow 2Mg^{2+} + 4e^-$

Overall: $2Mg + O^2 + 2H_2O \rightarrow 2Mg(OH)_2$

Fig. 1.

Structure and working principle of an Mg-air battery.

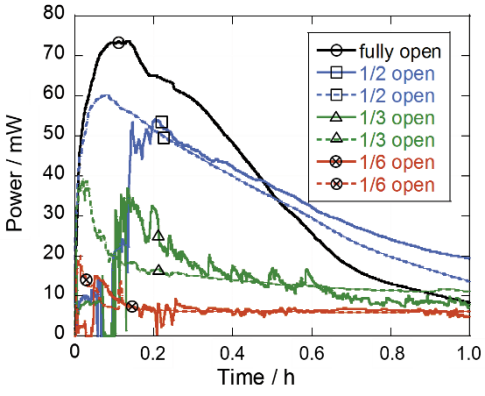

Fig. 2.

Discharge performance dependence on contact area when the initial water supply is 1.0 g.

* Specially Appointed Researcher
** Guest Professor
*** Specially Appointed Professor

Inorganic Chemistry, 54, 16 (2015), 7976-7984.
doi: 10.1021/acs.inorgchem.5b01112

Hydrothermal synthesis of yttria-stabilized zirconia nanocrystals with controlled yttria content

Kazuyoshi Sato*, Kazuya Horiguchi*, Taku Nishikawa*, Sadahiro Yagishita**, Kazuo Kuruma***, Takeshi Murakami***, Hiroya Abe****

Abstract

In this study, we demonstrate for the first time the hydrothermal synthesis of yttria-stabilized zirconia (YSZ) nanocrystals with controlled yttria content (x = 3–12 mol %; xYSZ) with negligible aggregation from aqueous solution. The nanocrystals were grown via the hydrothermal treatment of basic Zr(IV) and Y(III) carbonate complex aqueous solutions in the presence of a cationic ligand, $N(CH_3)_4^+$. The nanocrystals were characterized in detail by dynamic light scattering, ζ-potential measurement, X-ray diffraction, specific surface area measurement based on the Brunauer–Emmett–Teller theory, transmission electron microscopy, energy dispersive X-ray spectroscopy, and Raman spectroscopy. Shorter reaction times and higher Y_2O_3 content produce aqueous solutions with higher transparencies containing nanocrystals with sizes of 10 nm or less. Nanocrystals with the target composition were obtained by hydrothermal reaction for longer than 3 h, regardless of the Y_2O_3 content. The main phase is tetragonal for (3–6)YSZ and cubic with disordered oxygen vacancies for (8–12)YSZ. The characteristics of the nanocrystalline material synthesized are consistent with those of bulk YSZ crystals, indicating the growth of high-quality nanocrystals. (Reprinted with permission from K. Sato et al., *Inorg. Chem.*, 2015, 54, 7976-7984, Copyright 2015 American Chemical Society)

Keywords

Yttria- stabilized zirconia (YSZ); Nanocrystal; Hydrothermal; Cationic ligand; Carbonate complex

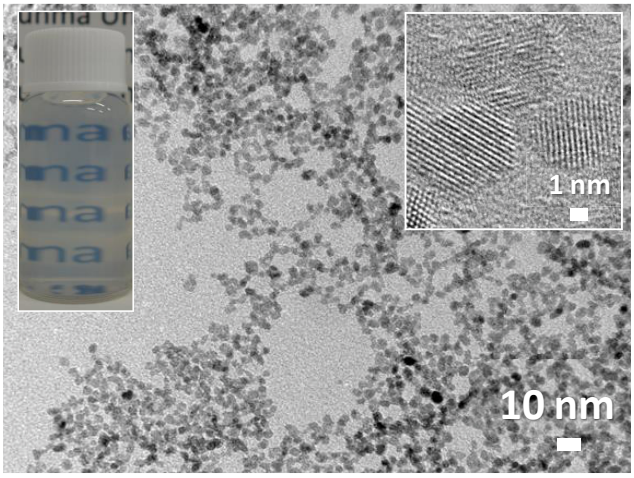

YSZ nanocrystals synthesized via the hydrothermal treatment of basic Zr(IV) and Y(III) carbonate complex aqueous solutions in the presence of a cationic ligand, $N(CH_3)_4^+$.

* Gunma University
** Daiichi Kigenso Kagaku Kogyo Co. Ltd.
*** Osaka University
**** Associate Professor

Mechanical Engineering Letters, 2, (2016), 15-00481.
doi: 10.1299/mel.15-00481

Experimental assessment of temperature distribution in heat affected zone (HAZ) in dissimilar joint between 8Cr-2W steel and SUS316L fabricated by 4 kW fiber laser welding

Sho Kano*, Akira Oba*, Huilong Yang*, Yoshitaka Matsukawa*, Yuhki Satoh*, Hisashi Serizawa**, Hideo Sakasegawa***, Hiroyasu Tanigawa*** and Hiroaki Abe*

Abstract

High-Cr steel (Fe-8Cr-2W-0.4Mn-0.2V-0.06Ta, so-called F82H steel) is one of the candidate structure materials for fusion blanket system, and its dissimilar welding technology to stainless steel (SUS316L) is an inevitable issue. Purpose of the present study is to identify the microstructure characteristics of dissimilar joint between F82H and SUS316L fabricated by fiber laser welding. The microstructure of as-welded specimens was composed of heat affected zone (coarse grain (CGHAZ) and fine grain (FGHAZ)) in F82H side, and weld metal (WM). Distributions of size, density and chemical composition of $M_{23}C_6$-type precipitates in HAZ were examined as a function of the distance from WM/HAZ interface. Besides, isochronal annealing experiments on F82H performed to obtain relationship between annealing temperature and Cr (or C) concentration in $M_{23}C_6$ precipitates. By comparison of their microstructure with that of HAZ, temperature distribution in HAZ upon welding was evaluated. It is suggested that the HAZ/F82H interface and the FGHAZ/CGHAZ boundary were heated up to 1150 K and 1400 K, respectively. Further applications of this method to clarify the temperature history and its distribution in HAZ, as well as increase in diagnostic accuracy, are greatly expected.

Keywords

Fiber laser welding; Dissimilar joint; F82H; SUS316L; $M_{23}C_6$; Temperature gradient; HAZ

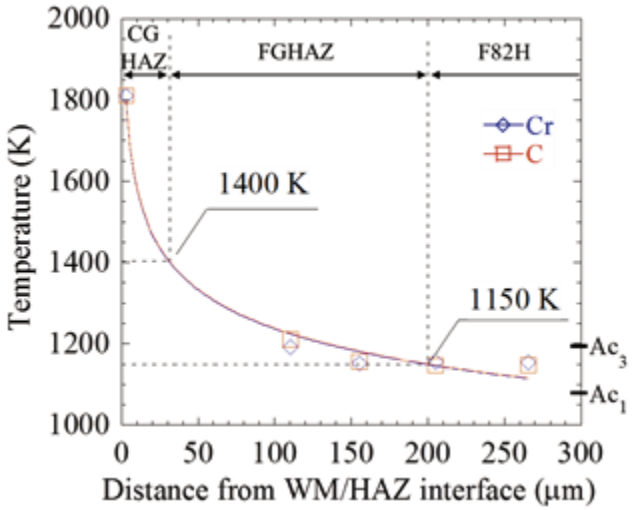

Fig. 1. Dependence of temperature under fiber laser welding on distance from WM/HAZ interface calculated by Cr/C concentration in $M_{23}C_6$ precipitate.

* Tohoku University
** Associate Professor
*** Japan Atomic Energy Agency

Nano Biomedicine, 7, 1 (2015), 11–20.
http://doi.org/10.11344/nano.7.11

Biological response to nanostructure of carbon nanotube/titanium composite surfaces

Erika Nishida*, Hirofumi Miyaji*, Junko Umeda***, Katsuyoshi Kondoh**, Hiroko Takita*, Izumi Kanayama*, Saori Tanaka*, Akihito Kato*, Bunshi Fugetsu****, Tsukasa Akasaka*, Masamitsu Kawanami*

Abstract

Titanium (Ti) is currently used in dental implants and bone fixation devices due to its high biocompatibility. Biomodification of the Ti surface up-regulates its biocompatibility. Reportedly, carbon nanotubes (CNTs) were available for biomedical applications, such as neuronal growth, bone induction and drug delivery. In this study, we fabricated the CNT-coated Ti and assessed its biocompatibility and bone forming ability.

Pure Ti plates were coated with multi-wall CNTs dispersions, and then annealed in a vacuum furnace to anchor the CNTs to the Ti plate. Comparison of cell morphology and viability of osteoblastic cell on the CNT-coated Ti was assessed using SEM and fluorescent microscopy. Subsequently, sample receiving bone morphogenetic protein-2 (BMP-2) was placed on the cranial bone of rat and histological analysis was carried out. Cell spreading and proliferation on the Ti plate were promoted by CNTs modification. In addition, remarkable cell viability was exhibited by application of low dose CNTs compared to high dose. In rat implantation test, CNTs and BMP-2 application stimulated new bone formation, however, the joint between bone and CNT-modified Ti was poor. Therefore, a more applicable method should be created for biomedical application.

Keywords

Titanium; Carbon nanotubes (CNTs); Surface modification; Biocompatibility; Cell proliferation; Biomaterials

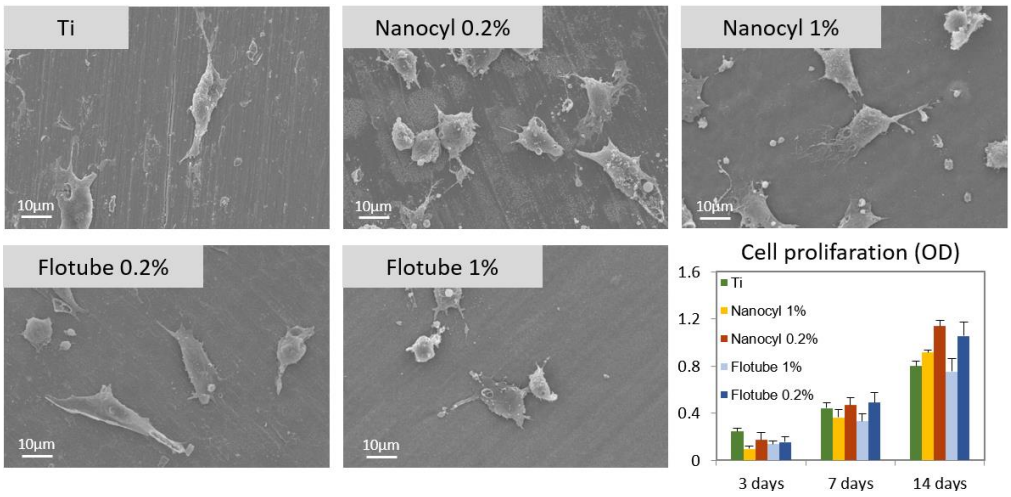

Fig. 1. Cell morphology and proliferation assay.

* Hokkaido University
** Professor
*** Associate Professor
**** The University of Tokyo